CHM 696-11: Week 7

Instructor: Alexander Wei

Supramolecular Chemistry of Metal Nanoparticles

Reviews:

Templeton et al, *Acc. Chem. Res.* **2000**, *33*, 27-36.

Daniel and Astruc, *Chem. Rev*. **2004**, *104*, 293-346

Over 660 references (but still incomplete!)

Metal nanocrystals: lattice structure

"Magic Number" Face-centered cubic (fcc) nanocrystals: Paragons of symmetry

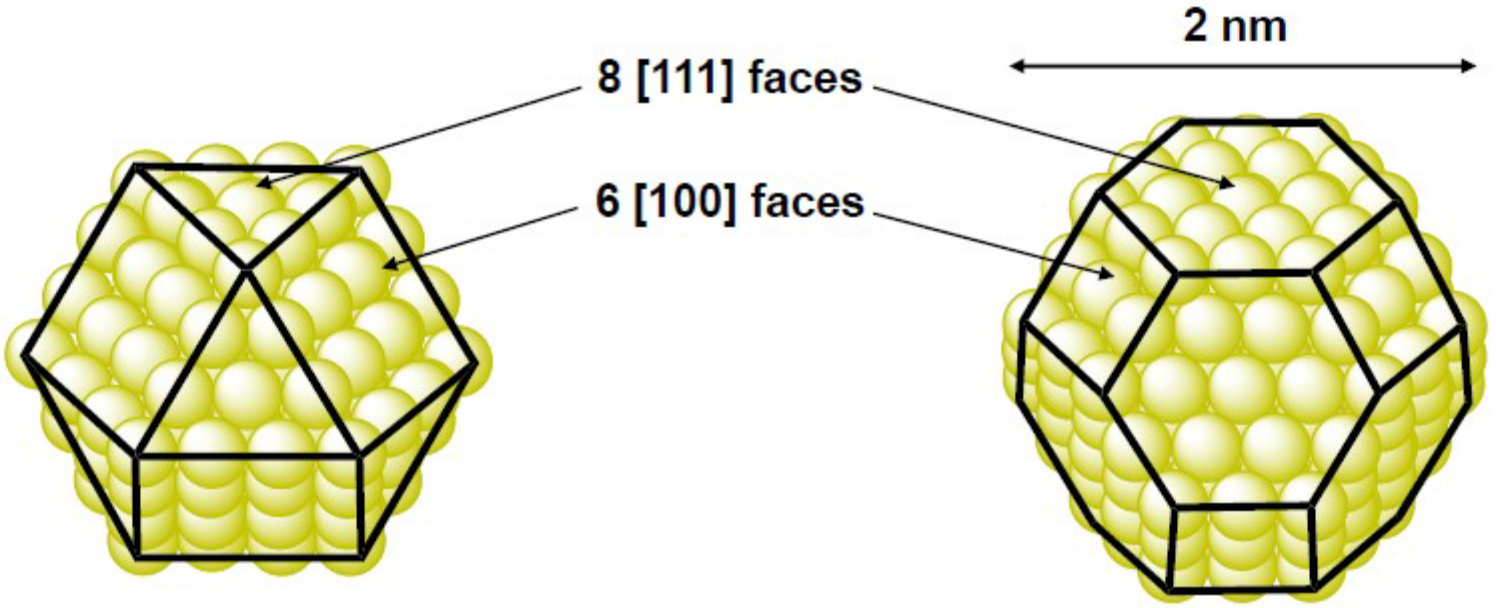

M_{147}: 3-shell fcc nanocrystal cuboctahedron

M_{203} truncated octahedron

Typical situation: polydispersity in shape and size

coefficient of variance below 10% is considered to be good

SAMs on Nanoparticles

Monolayer-protected clusters (MPCs): 1-5 nm

Ordered domains on (111) terraces:
all-*trans* conformation

Alkanethiols at NP edges and vertices:
gauche defects

Ordered/disorder ratio increases with MPC size

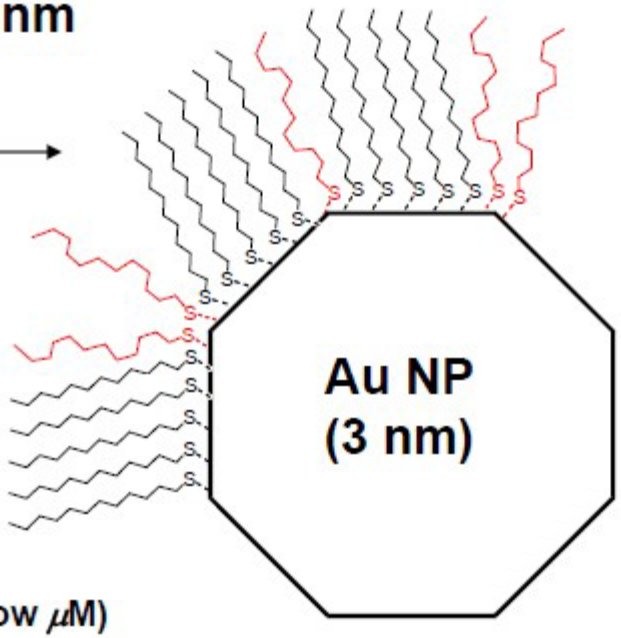

Concentration range: typically 10^{15}-10^{17} particles/mL (nM to low μM)

MPCs vs. SAMs on Au(111):

Similar chemical bonding (adsorbed species considered Au-thiolate)

Higher surfactant coverage (S/Au surface atom ratio > 50%, vs. 33% for SAMs on Au(111))

Greater disorder for MPCs → Faster ligand exchange rates

Templeton, Wuelfing, and Murray, *Acc. Chem. Res.* **2000**, *33*, 27.

Synthesis of MPCs: The Brust-Schiffrin method

Original biphasic reaction:

1) $AuCl_4^{-}$ (aq.) + $(C_8H_{17})_4N^+Br^-$ (TOA^+Br^-) → $AuCl_4^-TOA^+$ (soluble in organic solvents)

2) $AuCl_4^-$ TOA^+ + R-SH (org.) + $NaBH_4$ (aq.) → $Au_x(SR)_y$ (MPCs, 1-3 nm)

Brust et al, *Chem. Commun.* **1994**, 801.

"Thiol-free" recipe:

$AuCl_4^-$ TOA^+ (org.) + $NaBH_4$ (aq.) → $Au_x(X^-)_y[TOA^+]_z$ (3-5 nm Au particles)

Fink et al, *Chem. Mater.* **1998**, *10*, 922.

High-resolution TEM image of MPCs

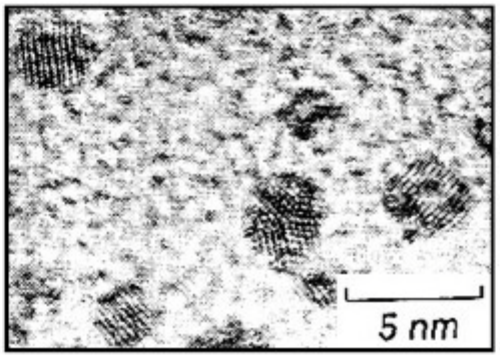

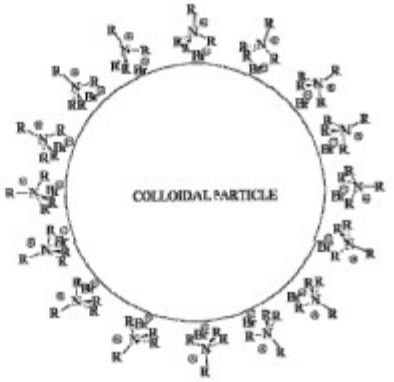

Size control in MPC synthesis

Ratio of $AuCl_4$: C12 thiol (Au/S) varied in Brust-Schiffrin reaction

Good size control for metal core diameters < 10 nm

D = diameter of Au metal core
R = radius of MPC (incl. thiol)

Leff et al, *J. Phys. Chem.* **1995**, *99*, 7036.

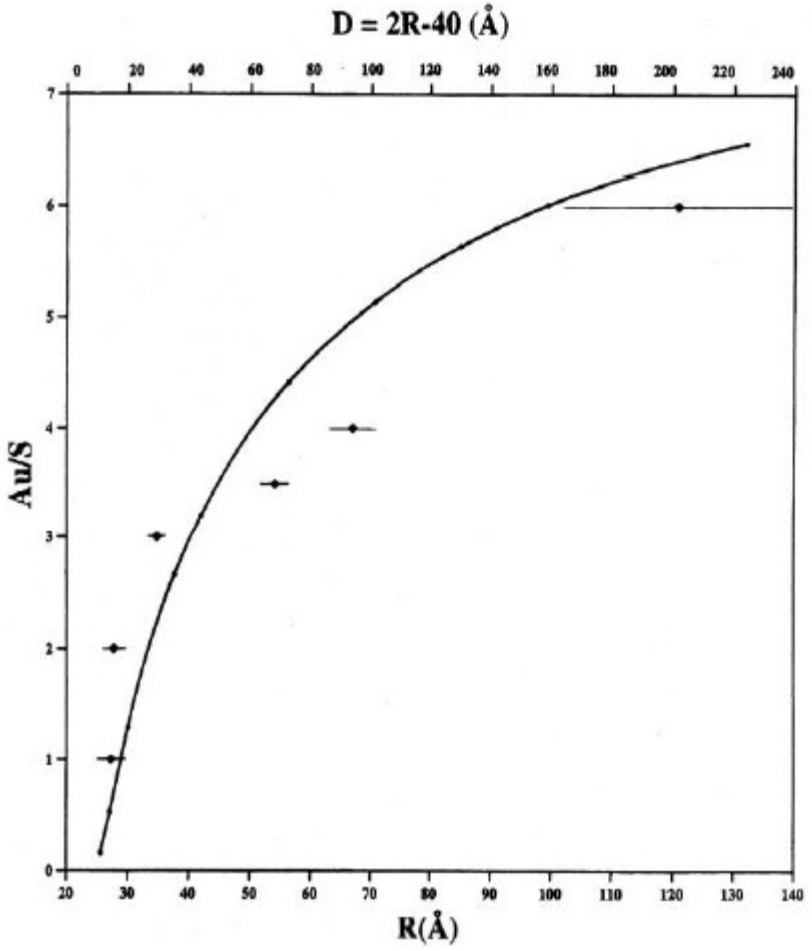

Chemical characterization of MPCs

The following analytical techniques are applicable to MPCs ≤ 5 nm:

Mass spectrometry: only for small MPCs ($< M_{500}$)

Elemental analysis: total S/Au ratio

XPS, thermogravimetric analysis (TGA): average ligand/surface Au atom ratio

Solution- and solid-state NMR: Structural and dynamic information of ligand

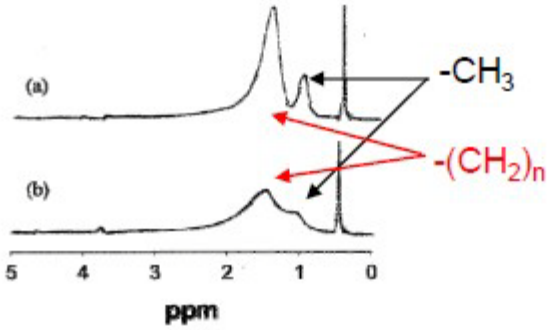

^{1}H NMR of C12-thiol MPCs. (a) 2-nm core; (b) 4.4-nm core.

Hostetler et al, *Langmuir* **1998**, *14*, 17.

Post-degradation chemometric analysis (applicable to larger sizes):

Ligand analysis by NMR (small MPCs), fluorescence (larger MPCs), or sensitive bioassay detections (biomolecular ligands)

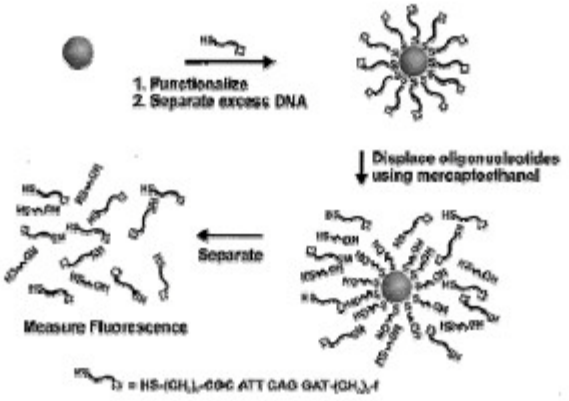

Demers et al, *Anal. Chem.* **2000**, *72*, 5535.

Chemical reactivity of Au MPCs

1) Ligand place exchange

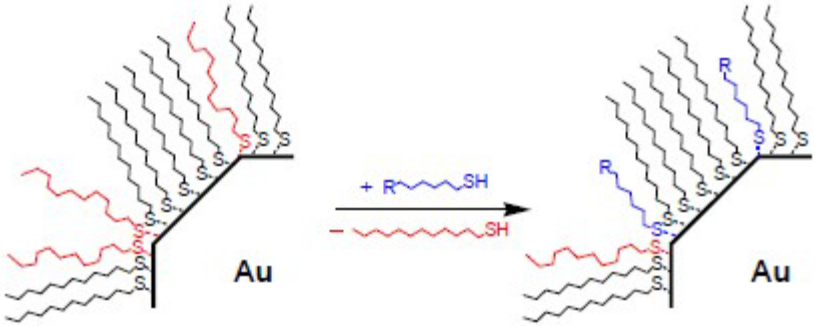

- Associative mechanism
- Occurs fastest at disordered sites
- Surface diffusion on MPC surface

(Rate of ligand exchange: ??)

3) Stability of Au core

- Au etching by I_2, CN^-
- MPC reshaping by organic surfactants

2) Covalent synthesis on MPCs

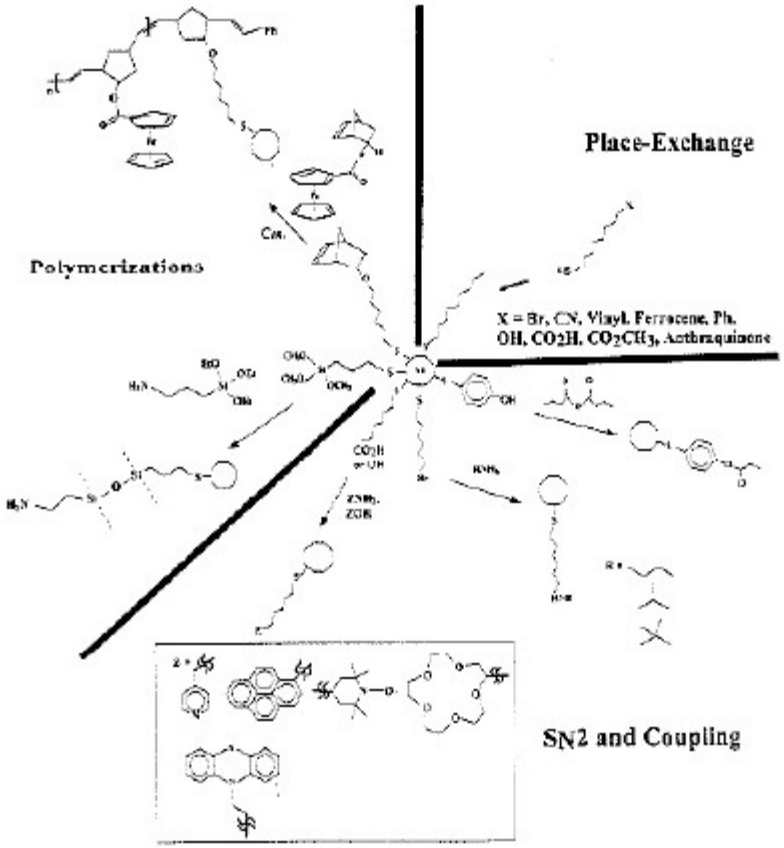

Templeton, Wuelfing, and Murray, *Acc. Chem. Res.* **2000**, *33*, 27.

Digestive ripening of Au MPCs

Au nanoparticles prepared without alkanethiols:

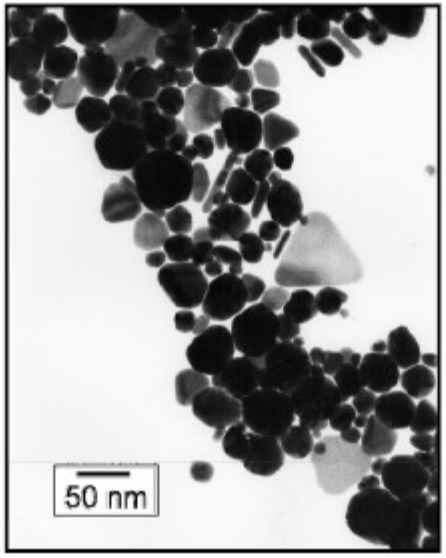

Au nanoparticles after digestive ripening with C12 thiol (Au/S = 1:30):

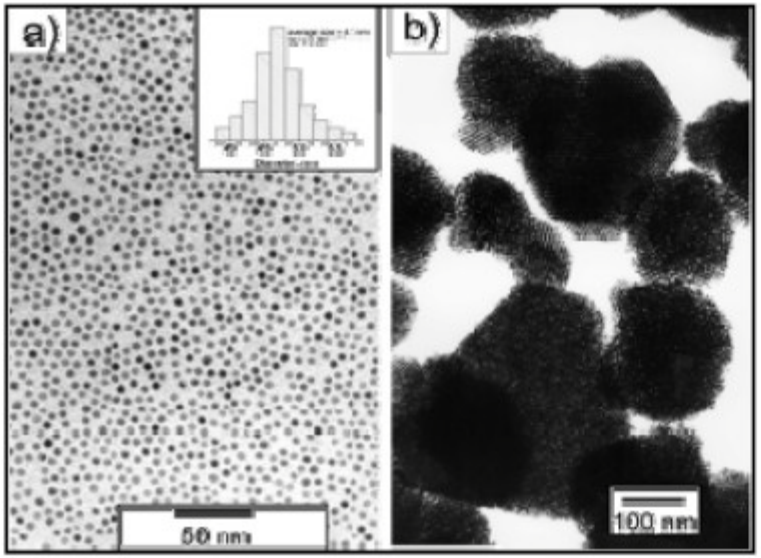

Particle size distributions by different digestive ripening agents:

C12-SH	4.7 ± 0.4 nm
C16-SH	5.5 ± 0.4 nm
$(C8)_3P$	7.1 ± 1.1 nm
$C18\text{-}SiH_3$	7.2 ± 1.0 nm
$C12\text{-}NH_2$	8.6 ± 1.3 nm

Prasad et al, *Langmuir* **2002**, *18*, 7515.
Prasad et al, *Chem. Mater.* **2003**, *15*, 935.

Electronic properties of metal nanoparticles: Size confinement effects

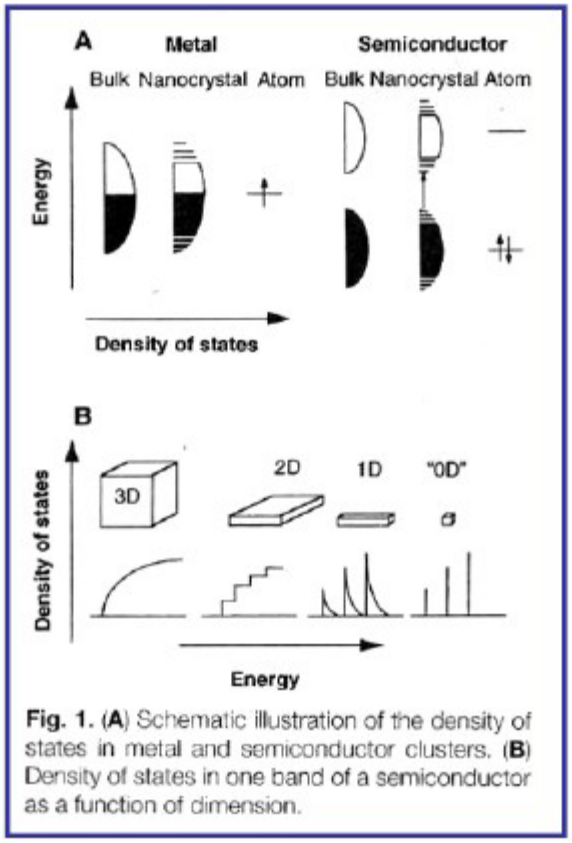

Fig. 1. (**A**) Schematic illustration of the density of states in metal and semiconductor clusters. (**B**) Density of states in one band of a semiconductor as a function of dimension.

Alivisatos, A. P. *Science* **1996**, *271*, 933

Electrochemical double-tunnel junction Based on a Au MPC

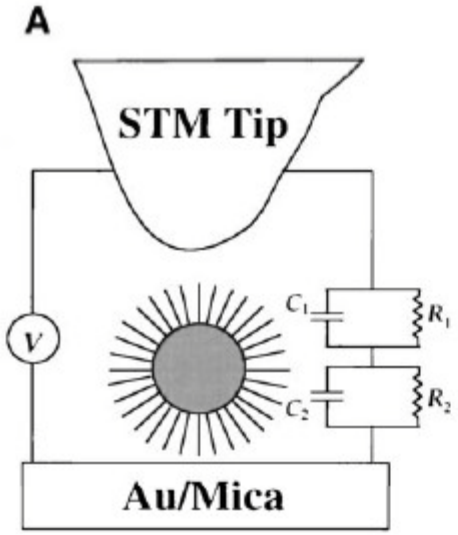

Quantized "Coulomb staircase" charging:

$E_C = e^2/C$

(observable at RT)

Double-layer capacitive charging steps should occur at regular voltage intervals:

$\Delta V_C = e/C$

Andres et al. *Science* **1996**, *272*, 1323.
Chen et al. *Science* **1998**, *280*, 2098.

Capacitive charging vs. redox-like properties

Cyclic voltammetry on Au MPCs:

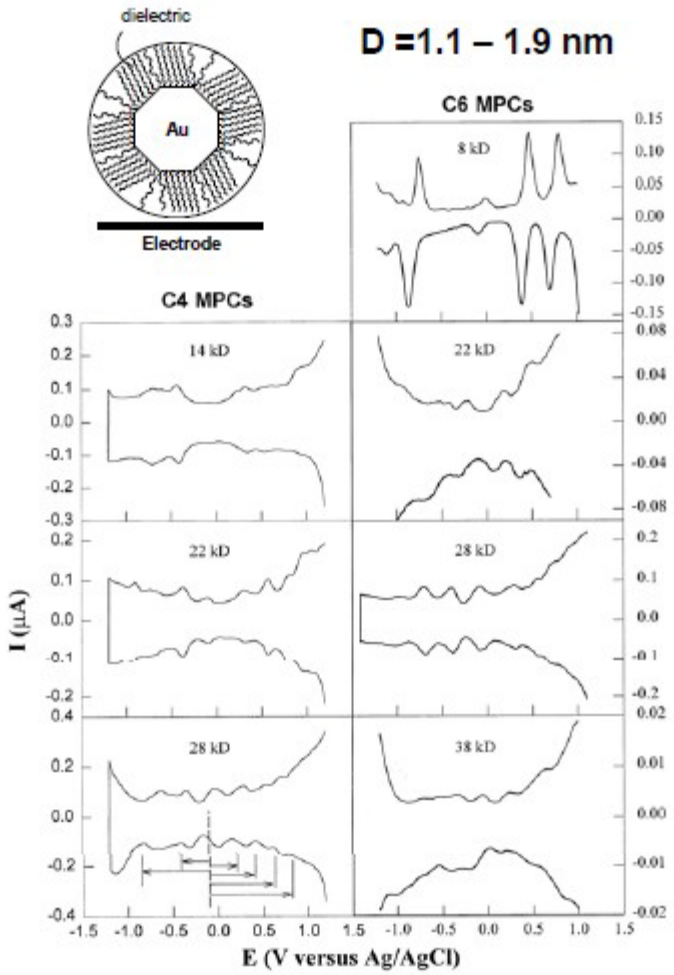

Redox-like behavior for 8, 14 kD MPC (HOMO–LUMO gap: ~0.4-0.9 eV)

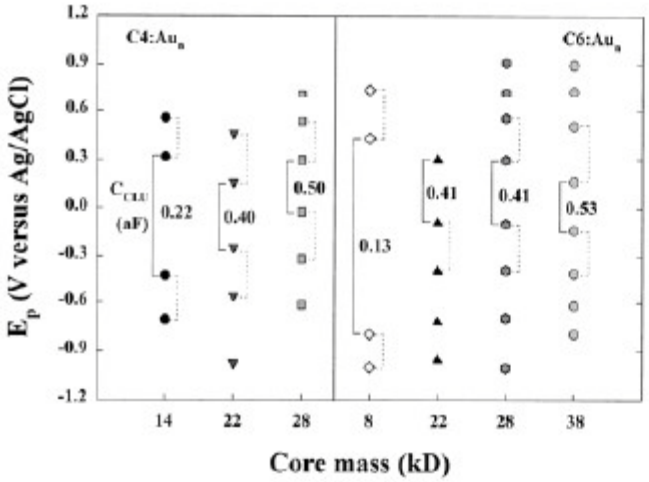

Consecutive charging steps: $\Delta V_C = e/C$

Lower capacitance for C4 MPCs: Larger charging steps observed for 28 kD MPC

Chen et al. *Science* **1998**, *280*, 2098.

Supramolecular chemistry on metal nanoparticles

Early example involving β-cyclodextrin heptathiol (1) as surface receptor: Ligand-mediated aggregation of 15-nm Au particles

Liu et al. *J. Am. Chem. Soc.* **1999**, *121*, 4304.

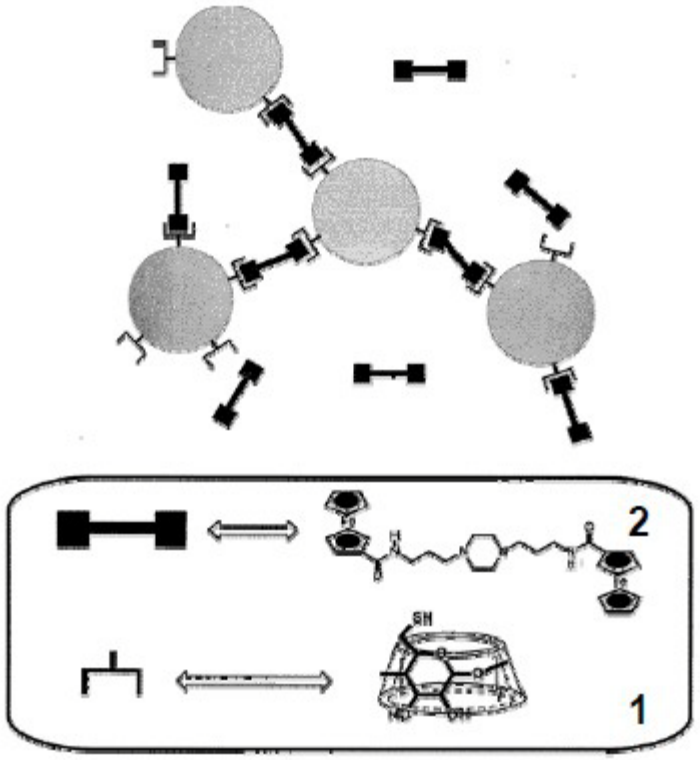

Time-dependent changes in plasmon resonance: loss due to precipitation of aggregated particles

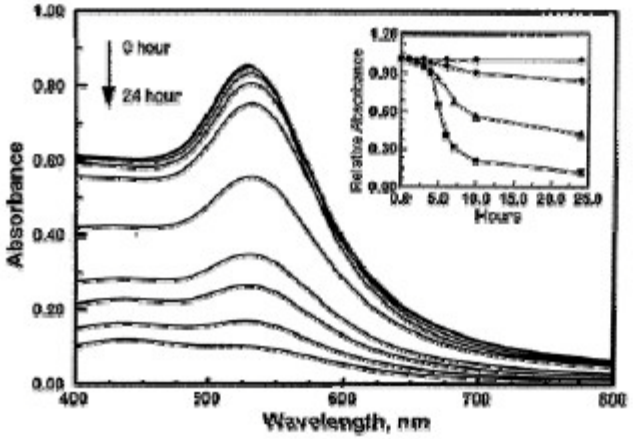

Absorption spectrum of colloidal dispersion modified by **1**, after addition of 0.1 mM dimer **2**.

Inset: Time dependence of the relative absorbance (at 526 nm) recorded after addition of 0.1 mM **2** (circles), 0.1 mM **2** + 0.1 mM β-CD (diamonds), 0.1 mM **2** + 1 mM β-CD, and 0.1 mM **2** + 6 mM β-CD (squares).

MPCs as scaffolds: supramolecular sensors

Recognition of reduced flavin by functionalized MPC:

Boal and Rotello, *JACS* **1999**, 4914.

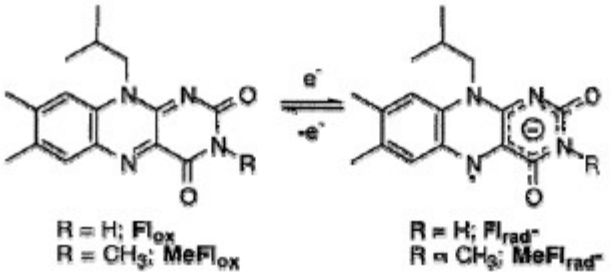

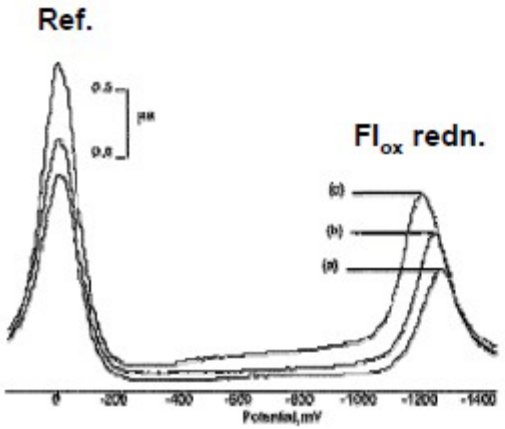

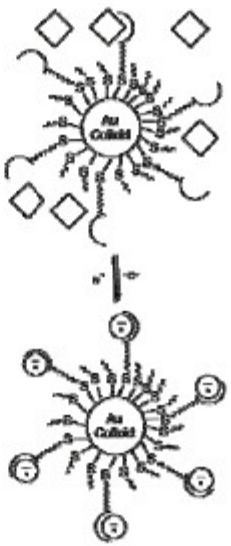

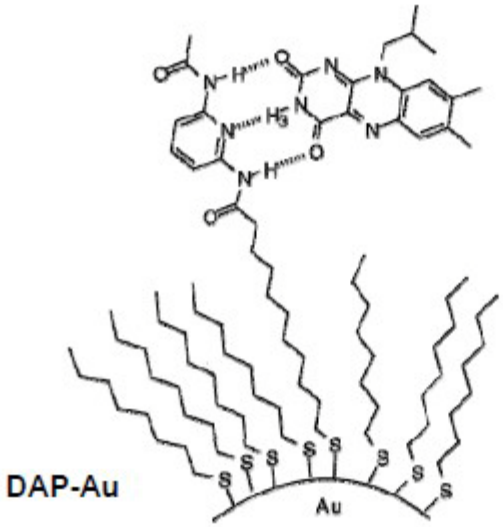

Change in **Fl$_{ox}$**/**Fl$_{rad}$-** redox couple upon addition of **DAP-Au**.

(a): 0 equiv **DAP-Au**, $E_{1/2}$ **Fl$_{ox}$** = -1260 mV (vs. ferrocene);

(b): 83 equiv **DAP-Au**, $E_{1/2}$ **Fl$_{ox}$** = -1222 mV;

(c): 96 equiv **DAP-Au**, $E_{1/2}$ **Fl$_{ox}$** = -1184 mV.

$\Delta E_{1/2}$ **Fl$_{ox}$** = 85 mV; stabilization of **Fl$_{rad}$-** = 1.85 kcal/mol

No change in $E_{1/2}$ for **MeFl$_{ox}$**

20-fold increase in binding of **Fl$_{rad}$-** over **Fl$_{ox}$-**